Small Target Detection Improvement in Hyperspectral Image

Tao Lin, Julien Marot, and Salah Bourennane

Institut Fresnel / CNRS-UMR 7249
Ecole Centrale Marseille, Aix-Marseille Université
13013 MARSEILLE, France

Abstract. Target detection is an important issue in the HyperSpectral Image (HSI) processing field. However, current spectral-identification-based target detection algorithms are sensitive to the noise and most denoising algorithms cannot preserve small targets, therefore it is necessary to design a robust detection algorithm that can preserve small targets. This paper utilizes the recently proposed multidimensional wavelet packet transform with multiway Wiener filter (MWPT-MWF) to improve the target detection efficiency of HSI with small targets in the noise environment. The performances of the our method are exemplified using simulated and real-world HSI.

Keywords: Hyperspectral image, small target detection, multiway Wiener Filter.

1 Introduction

HSI consists of spatial locations and spectral signatures [4]. The additional spectral signature information makes it a suitable tool for target detection in many military and civilian applications, such as military vehicle detection and mine detection [15]. However, the HSI is always impaired by noise from radiation, atmospheric scattering and thermal noise in the sensor instrument [10], which can degrade the detection performances, therefore it is necessary to use denoising techniques for improving the detection efficiencies.

The classical denoising methods rearrange the HSI into a matrix whose columns contain the spectral signatures of all the pixels and principal component analysis (PCA) is used to estimate the signal subspace [17]. These methods own the convenience of using matrix algebra, however they neglect the HSI data structure which also contains useful information. To preserve the data structure, a multiway Wiener filter (MWF) [3, 12, 13, 16] is proposed to process a HSI as a whole entity based on TUCKER3 decomposition [7, 8]. In MWF, the filter in each mode is computed as a function of the filters in other modes, which reflects its capability in integrally utilizing the information in each mode of the multidimensional data.

Though MWF preserves the data structure of HSI, it also has some negative side effects in preserving small targets in the denoising process. In fact,

J. Blanc-Talon et al. (Eds.): ACIVS 2013, LNCS 8192, pp. 460–469, 2013.

MWF is essentially an optimal low-pass filter while small targets are high frequency signals in Fourier basis, therefore MWF might remove small targets in the denoising process. A multidimensional wavelet packet transform with multidimensional Wiener filter (MWPT-MWF) is recently proposed to reduce noise in a jointly filtering component way [14]. It decomposes the HSI into different coefficient tensors (components) by wavelet packet transform [6], and jointly filter each component by MWF. In [14], we have discussed the SNR improvement performance of MWPT-MWF. In the subsequent study, we find MWPT-MWF also performs well in preserving small targets in the denoising process. In fact, since large target and small target are separated into different components, the latter can be preserved in the denoising process.

Since small target detection is an important issue in the HSI processing field [1, 11], in this paper, MWPT-MWF is used to reduce noise in HSI with small targets and hence improve the target detection performances in the noise environment. The experiments of simulated and real-world images are given to present the performances of target detection after denoising by MWPT-MWF.

The remainder of the paper is as follows: Section 2 introduces some basic knowledge about the multilinear algebra. Section 3 introduces the signal model. Section 4 shows how to use MWF to jointly filter the data component tensor. Section 5 presents some experimental results and finally section 6 concludes this paper.

2 Multilinear Algebra Tools

2.1 *n*-mode Unfolding

$\mathbf{X}_n \in \mathbb{R}^{I_n \times M_n}$ denotes the n-mode unfolding matrix [5] of a tensor $\mathcal{X} \in \mathbb{R}^{I_1 \times \ldots \times I_N}$, where $M_n = I_{n+1} \ldots I_1 I_N \ldots I_{n-1}$. The columns of $\mathbf{X}_n$ are the I_n-dimensional vectors obtained from $\mathcal{X}$ by varying index i_n while keeping the other indices fixed. Here, we define the n-mode rank K_n as the n-mode unfolding matrix rank, *i.e.*, $K_n = \text{rank}\,(\mathbf{X}_n)$.

2.2 *n*-mode Product

The n-mode product [5] is defined as the product between a data tensor $\mathcal{X} \in \mathbb{R}^{I_1 \times \ldots \times I_N}$ and a matrix $\mathbf{B} \in \mathbb{R}^{J \times I_n}$ in mode n. It is denoted by $\mathcal{C} = \mathcal{X} \times_n \mathbf{B}$, whose entries are given by $c_{i_1 \ldots i_{n-1} j i_{n+1} \ldots i_N} \triangleq \sum_{i_n=1}^{I_n} x_{i_1 \ldots i_{n-1} i_n i_{n+1} \ldots i_N} b_{j i_n}$ where $\mathcal{C} \in \mathbb{R}^{I_1 \times \ldots \times I_{n-1} \times J \times \ldots \times I_N}$

3 Signal Model

A noisy HSI is modeled as a tensor $\mathcal{R} \in \mathbb{R}^{I_1 \times I_2 \times I_3}$ resulting from a pure HSI $\mathcal{X} \in \mathbb{R}^{I_1 \times I_2 \times I_3}$ impaired by an additive noise $\mathcal{N} \in \mathbb{R}^{I_1 \times I_2 \times I_3}$. The tensor $\mathcal{R}$ can be expressed as:

$$\mathcal{R} = \mathcal{X} + \mathcal{N} \tag{1}$$

In this paper, only the thermal noise is considered, which means that the noise is modeled as independent white Gaussian noise with noise variance σ.

4 Noise Reduction by Joint Component Filtering

4.1 Multidimensional Wavelet Packet Transform

By performing wavelet packet transform (WPT) in each mode, the multidimensional wavelet packet transform (MWPT) can be written in tensor form as:

$$\mathcal{C}^R = \mathcal{R} \times_1 \mathbf{W}_1 \times_2 \mathbf{W}_2 \times_3 \mathbf{W}_3 \tag{2}$$

and the reconstruction can be written as:

$$\mathcal{R} = \mathcal{C}^R \times_1 \mathbf{W}_1^T \times_2 \mathbf{W}_2^T \times_3 \mathbf{W}_3^T \tag{3}$$

where $\mathbf{W}_n \in \mathbb{R}^{I_n \times I_n}, n = 1, 2$ indicate the wavelet packet transform matrices. When the transform level vector is $\mathbf{l} = [l_1, l_2, l_3]^T$, where $l_n \geq 0$ denotes the wavelet packet transform level in mode n, the coefficient tensor $\mathcal{C}^{\mathcal{R}}_{\mathbf{l},\mathbf{m}}$, which is also called a component in this paper, of scale $\mathbf{m} = [m_1, m_2, m_3]$, where $0 \leq m_n \leq 2^{l_k} - 1$, can be extracted by:

$$\mathcal{C}^{\mathcal{R}}_{\mathbf{l},\mathbf{m}} = \mathcal{C}^R \times_1 \mathbf{E}_{m_1} \times_2 \mathbf{E}_{m_2} \times_3 \mathbf{E}_{m_3} \tag{4}$$

and the corresponding inverse process is:

$$\mathcal{C}^R = \sum_{m_1} \sum_{m_2} \sum_{m_3} \mathcal{C}^{\mathcal{R}}_{\mathbf{l},\mathbf{m}} \times_1 \mathbf{E}_{m_1}^T \times_2 \mathbf{E}_{m_2}^T \times_3 \mathbf{E}_{m_3}^T \tag{5}$$

where the extraction operator $\mathbf{E}_{m_n}$ is defined as:

$$\mathbf{E}_{m_n} = [\mathbf{0}_1, \mathbf{I}_{\frac{I_n}{2^{l_n}} \times \frac{I_n}{2^{l_n}}}, \mathbf{0}_2] \in \mathbb{R}^{I_n / 2^{l_n} \times I_n} \tag{6}$$

where $\mathbf{0}_1$ is a zero matrix with size $\frac{I_n}{2^{l_n}} \times \frac{m_n I_n}{2^{l_n}}$ and $\mathbf{0}_2$ is a zero matrix with size $\frac{I_n}{2^{l_n}} \times \frac{(2^{l_n} - 1 - m) I_n}{2^{l_n}}$.

4.2 Joint Component Filtering

As proposed in [14], the signal coefficient tensor $\mathcal{C}^{\mathcal{X}}_{\mathbf{l},\mathbf{m}}$ can be estimated by filtering the noisy data coefficient tensor $\mathcal{C}^{\mathcal{R}}_{\mathbf{l},\mathbf{m}}$ with MWF.

$$\hat{\mathcal{C}}^{\mathcal{X}}_{\mathbf{l},\mathbf{m}} = \mathcal{C}^{\mathcal{R}}_{\mathbf{l},\mathbf{m}} \times_1 \mathbf{H}_{1,\mathbf{m}} \times_2 \mathbf{H}_{2,\mathbf{m}} \times_3 \mathbf{H}_{3,\mathbf{m}} \tag{7}$$

where $\mathbf{H}_{n,\mathbf{m}}$ is the mode-n MWF filter:

$$\mathbf{H}_{n,\mathbf{m}} = \mathbf{V}^{(n)}_{s,\mathbf{m}} \mathbf{\Lambda}^{\gamma}_{\mathbf{m}} \left[\mathbf{\Lambda}^{\Gamma}_{\mathbf{m}} + \sigma_n^{\Gamma 2} \mathbf{I}_{K_n} \right]^{-1} {\mathbf{V}^{(n)}_{s,\mathbf{m}}}^T \tag{8}$$

where $\mathbf{V}^{(n)}_{s,\mathbf{m}}$ is the n-mode signal subspace basis, $\mathbf{\Lambda}^{\gamma}_{\mathbf{m}}$ and $\mathbf{\Lambda}^{\Gamma}_{\mathbf{m}}$ are the eigenvalues of $\gamma^{(n)}_{RR} = E\left[\mathbf{C}^{\mathcal{R}}_n \mathbf{q}^{(n)} {\mathbf{C}^{\mathcal{R}}_n}^T\right]$ and $\Gamma^{(n)}_{RR} = E\left[\mathbf{C}^{\mathcal{R}}_n \mathbf{Q}^{(n)} {\mathbf{C}^{\mathcal{R}}_n}^T\right]$ respectively, and $\sigma_n^{\Gamma 2}$

is the n-mode noise variance which can be estimated as the mean of the $I_n - K_n$ smallest eigenvalues of $\Gamma_{RR}^{(n)}$ with K_n the rank of $\gamma_{RR}^{(n)}$.

After each signal coefficient tensor being estimated, the signal estimate can be obtained by:

$$\hat{\mathcal{X}} = \hat{\mathcal{C}}^{\mathcal{X}} \times_1 \mathbf{W}_1^T \times_2 \mathbf{W}_2^T \times_3 \mathbf{W}_3^T \tag{9}$$

where

$$\hat{\mathcal{C}}^{\mathcal{X}} = \sum_{m_1} \sum_{m_2} \sum_{m_3} \hat{\mathcal{C}}_{\mathbf{l},\mathbf{m}}^{\mathcal{X}} \times_1 \mathbf{E}_{m_1}^T \times_2 \mathbf{E}_{m_2}^T \times_3 \mathbf{E}_{m_3}^T \tag{10}$$

Notice that the large and small targets are separated into the approximation and detail coefficient tensors respectively, which makes it possible to avoid removing the small target in filtering noise. Therefore, MWPT-MWF outperforms MWF in preserving the small targets.

5 Experimental Results

In the experiments, MWPT-MWF and MWF are compared in the aspect of improving target detection performances. The results obtained both on simulated and real-world data are presented in this section. The HSI is modeled as a three-dimensional tensor, where the first two dimensions indicate the spatial field and the third dimension indicates the spectral bands. Wavelet db3 is used to do MWPT-MWF with transform levels $[l_1, l_2, l_3] = [1, 1, 0]$.

SAM detector [9] is used in the experiments to detect targets in the image. As Spectral Angle Mapper (SAM) does not require the characterization of background, it can avoid the inaccuracy of the comparison result caused by the noise covariance matrix estimation error. The SAM detector can be expressed as:

$$\mathrm{T_{SAM}}(\mathbf{x}) = \frac{\mathbf{s}^T\mathbf{x}}{(\mathbf{s}^T\mathbf{s})^{1/2}(\mathbf{x}^T\mathbf{x})^{1/2}} \tag{11}$$

where $\mathbf{s}$ is the reference spectrum, $\mathbf{x}$ is the pixel spectrum. To assess the performances of detection, the probability of detection (Pd) is defined as:

$$\mathrm{Pd} = \frac{\sum_i^{n_s} N_i^{rd}}{\sum_i^{n_s} N_i} \tag{12}$$

and the probability of false alarm (Pfa) is defined as:

$$\mathrm{Pfa} = \frac{\sum_i^{n_s} N_i^{fd}}{\sum_i^{n_s} (I_1 \times I_2 - N_i)} \tag{13}$$

where n_s is the number of spectral signatures, N_i the number of pixels with spectral signature i, N_i^{rd} the number of rightly detected pixels, and N_i^{fd} the number of falsely detected pixels.

5.1 Results on Simulated Data

The simulated data is generated with the spectral signatures presented in Fig. 1 and it has 100 rows, 100 columns and 220 spectral bands, which can be modeled as a $100 \times 100 \times 220$ tensor. There are six target types and three different spatial sizes 9×9, 3×3, 1×1 of each type, which are shown in Fig. 2(a). These targets are mixed to the background by using the linear mixing model with target abundance being 80%. The band 6 of the noisy image with SNR=20dB is shown Fig. 2(b), from which one can see that the small targets are almost disappeared in the noise.

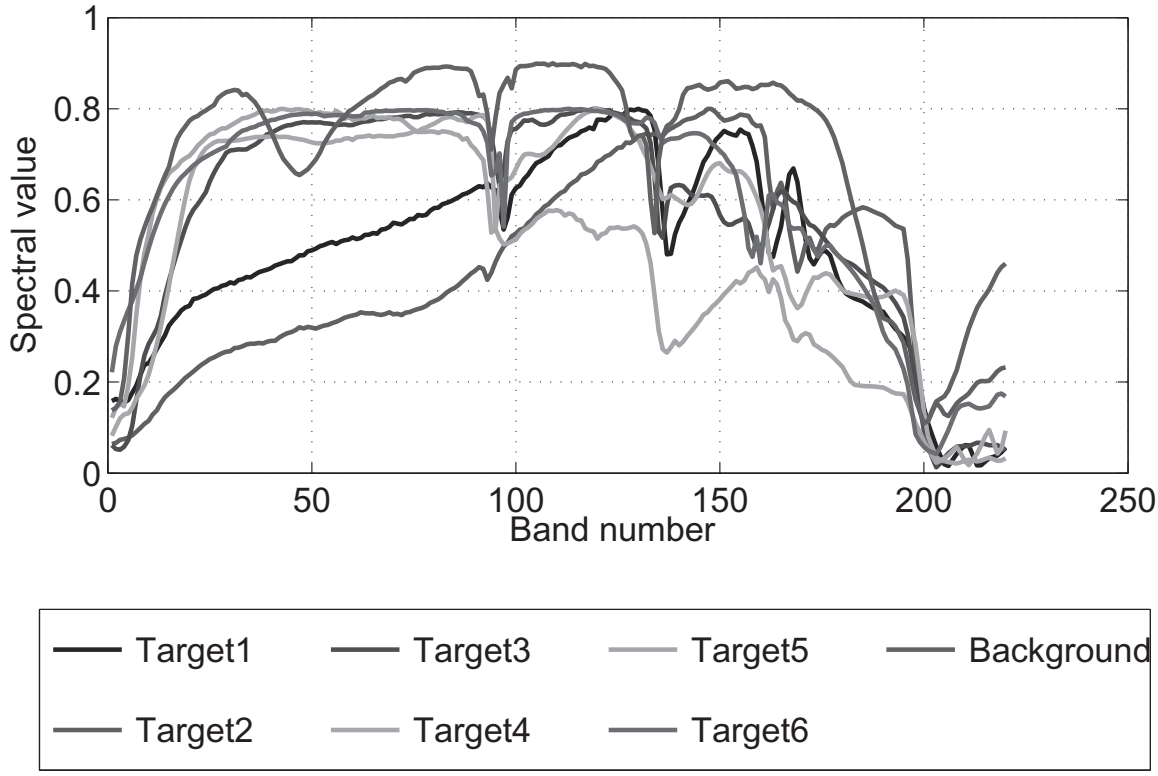

Fig. 1. Spectral signatures of the simulated data

Fig. 2(c) shows the detection result under Pfa $= 10^{-4}$ after denoising by MWF. In this figure, it is obvious that most of the 1×1 targets are not detected and there are two false alarm neighbors with the detected 1×1 targets. On the contrast, the detection result after denoising by MWPT-MWF is much better. The 2×2 targets are all detected and only one 1×1 target is dismissed. The experiment result in Fig. 2 implies that MWPT-MWF owns the capability in preserving the small targets in the denoising process.

To make the experimental results more convincing and show the subtle changes of the detection results, the receiver operating characteristic (ROC) values are given in Table 1 in the noise environments from 15dB to 25dB. In 15dB, Pd after denoising by MWPT-MWF is much greater than that by MWF under the same

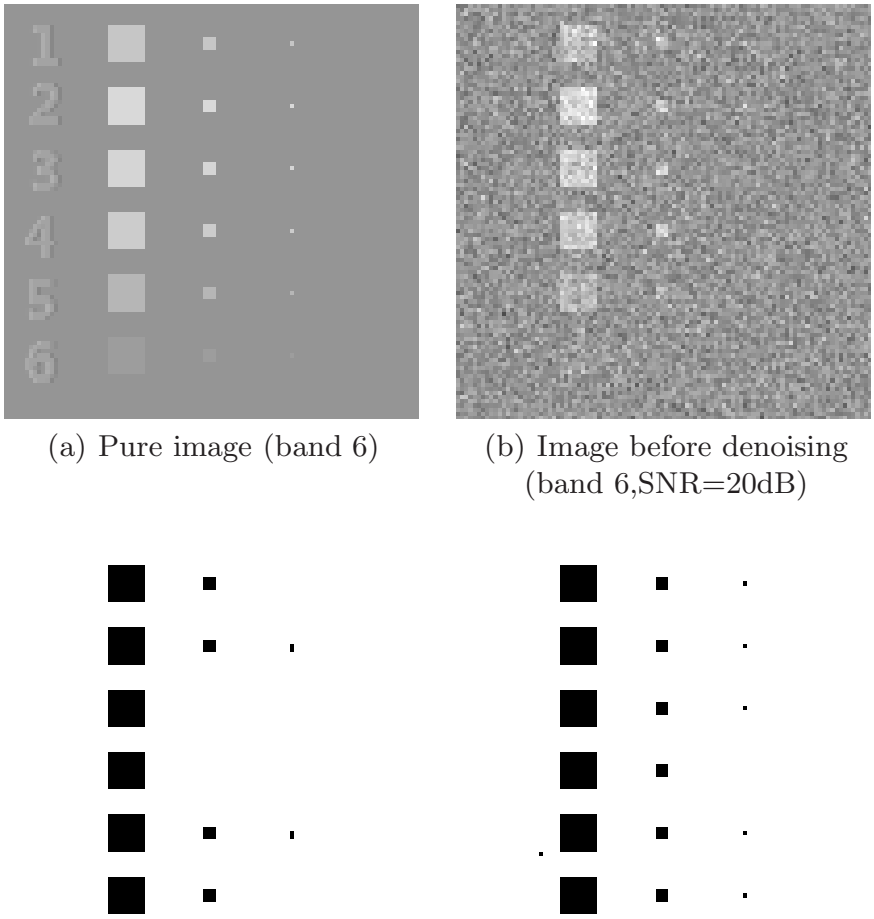

(a) Pure image (band 6)

(b) Image before denoising (band 6,SNR=20dB)

(c) Image denoised by MWF

(d) Image denoised by MWPT-MWF

Fig. 2. Detection results of HYDICE, Pfa=10^{-4}

Table 1. ROC values of MWF and MWPT-MWF for the simulated HSI

	Pd of MWF			Pd of MWPT-MWF		
Pfa	15dB	20dB	25dB	15dB	20dB	25dB
0.0001	0.5458	0.9597	0.9963	0.7125	0.9982	1.0000
0.0002	0.5714	0.9597	0.9963	0.7271	0.9982	1.0000
0.0003	0.5897	0.9597	0.9963	0.7381	0.9982	1.0000
0.0005	0.6190	0.9597	0.9982	0.7637	1.0000	1.0000
0.0008	0.6630	0.9597	0.9982	0.7821	1.0000	1.0000
0.0013	0.7088	0.9615	0.9982	0.8004	1.0000	1.0000
0.0022	0.7271	0.9615	0.9982	0.8132	1.0000	1.0000
0.0036	0.7601	0.9615	0.9982	0.8462	1.0000	1.0000
0.0060	0.8059	0.9689	0.9982	0.8956	1.0000	1.0000
0.0100	0.9011	0.9945	1.0000	0.9908	1.0000	1.0000

Pfa. From the comparison of ROC in Table 1, it shows that MWPT-MWF can improve the target detection performances more greatly than MWF can in different noise environments.

5.2 Results on Real-World Data

One high spatial resolution HSI HYDICE [2] is denoised by MWF and MWPT-MWF to compare their target detection improvement ability in noise environment. The HYDICE image contains 100 rows, 100 columns and 158 spectral bands, which is modeled as a $100 \times 100 \times 158$ tensor. Three types of target spectral signatures are considered, and these targets are mixed to the background with respect to the linear mixing model when target abundance is 80%;

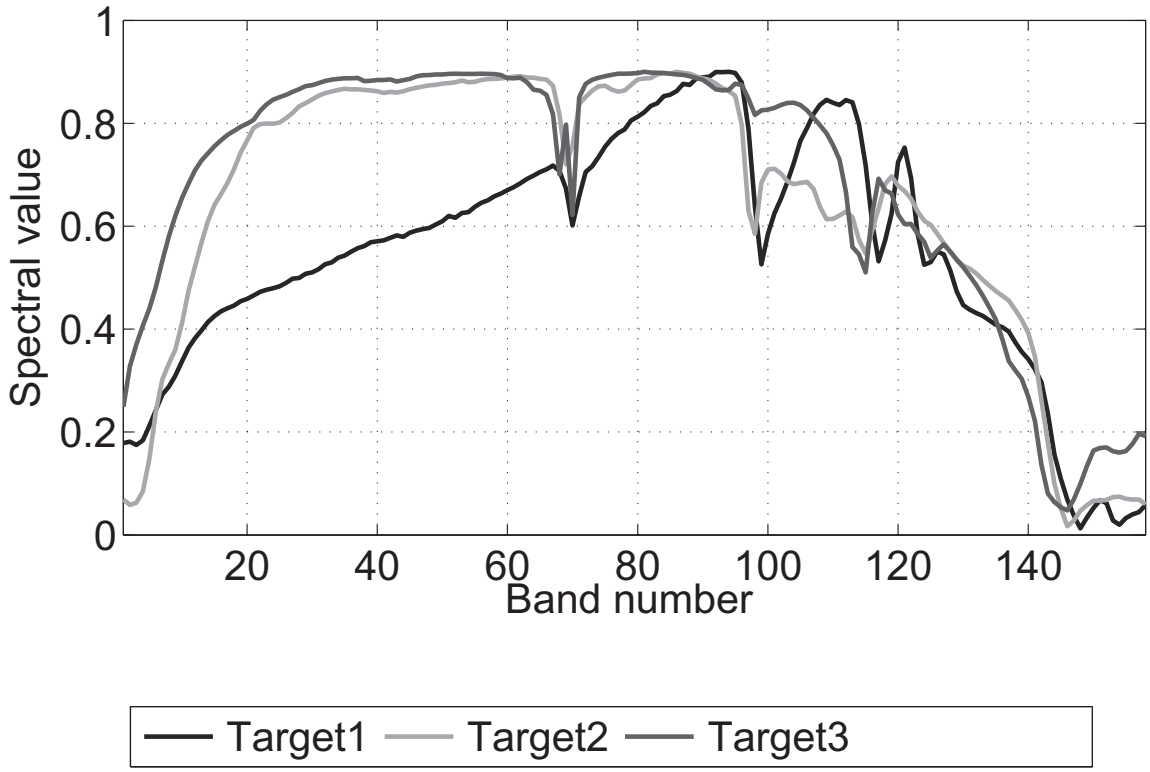

Fig. 3. Spectral signatures of targets

Fig. 4(a) and Fig. 4(d) are the pure and noisy images in band 50. The targets are placed in the field, beside the road and in the trees respectively to contain the usual target situations in HSI. The detection results after denoising by MWF and MWPT-MWF are shown in Fig. 4(c) and Fig. 4(d) respectively. In Fig. 4(d), 1×1 targets in the field and beside the road are detected. The only dismissed 1×1 target is in the trees, which is always a difficult situation to detect small target in it. On the contrast, in Fig. 4(c) all the 1×1 targets are dismissed and a 2×2 target in the trees is also lost. The comparison between Fig. 4(c) and Fig. 4(d) shows that MWPT-MWF owns better capability in preserving small targets than MWF as expected.

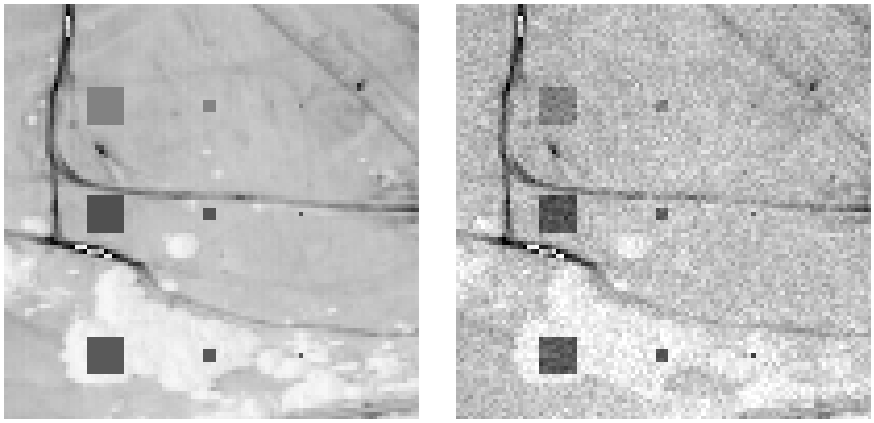

(a) Pure image (band 50)

(b) Image before denoising (band 50,SNR=20dB)

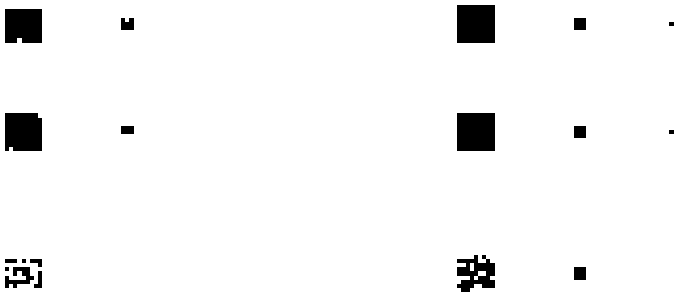

(c) Image denoised by MWF

(d) Image denoised by MWPT-MWF

Fig. 4. Detection results of HYDICE, Pfa=10^{-4}

Table 2. ROC values of MWF and MWPT-MWF for HYDICE

	Pd of MWF			Pd of MWPT-MWF		
Pfa	15dB	20dB	25dB	15dB	20dB	25dB
0.0001	0.6593	0.8828	1.0000	0.7289	0.8851	1.0000
0.0002	0.6593	0.9048	1.0000	0.7399	0.9084	1.0000
0.0003	0.6630	0.9121	1.0000	0.7546	0.9451	1.0000
0.0005	0.6703	0.9121	1.0000	0.7912	0.9634	1.0000
0.0008	0.6740	0.9487	1.0000	0.7985	0.9670	1.0000
0.0013	0.6777	0.9634	1.0000	0.8315	0.9707	1.0000
0.0022	0.6850	0.9780	1.0000	0.8498	0.9853	1.0000
0.0036	0.6923	1.0000	1.0000	0.8755	0.9927	1.0000
0.0060	0.7106	1.0000	1.0000	0.9341	0.9927	1.0000
0.0100	1.0000	1.0000	1.0000	1.0000	1.0000	1.0000

Apart from the binary target detection results in Fig. 4, to better compare the performances of MWF and MWPT-MWF, the ROC values are also presented in Table 2. As expected, the Pd of MWPT-MWF is better than that of MWF in the same Pfa. The comparison of the ROC values implies that MWPT-MWF performs better than MWF in improving the target detection result of the real-world data as well.

6 Conclusion

The performances of MWF and MWPT-MWF in improving the target detection in the noise environment are discussed in this paper. Though MWF performs well in reducing noise in HSI, it might also remove targets in the image, especially when the target is small. The reason leading to this phenomenon is that MWF treats directly HSI as a whole entity by filtering each mode of the HSI in a Wiener filter like way. Since the energy of the small target is thin, it is easy to be removed in the filtering process. However, MWPT-MWF decompose the HSI into several components (coefficient tensors) and filter each one by MWF. As small and large targets are separated into different components, the small ones can be preserved in the filtering process. This is why MWPT-MWF performs better than MWF in improving target detection performance when there exist small targets in the image.

Simulated and real-world HSIs are considered in the experiments to compare the performances of MWF and MWPT-MWF in improving target detection in the noise environment. The experimental results highlight that MWPT-MWF outperforms MWF in improving the target detection results in the presence of small targets.

References

1. Acito, N., Diani, M., Corsini, G.: A new algorithm for robust estimation of the signal subspace in hyperspectral images in the presence of rare signal components. IEEE Trans. Geosci. Remote Sens. 47(11), 3844–3856 (2009)
2. Basedow, R.W., Carmer, D.C., Anderson, M.E.: Hydice system: Implementation and performance. In: SPIE's 1995 Symposium on OE/Aerospace Sensing and Dual Use Photonics, pp. 258–267. International Society for Optics and Photonics (1995)
3. Bourennane, S., Fossati, C., Cailly, A.: Improvement of classification for hyperspectral images based on tensor modeling. IEEE Geosci. Remote Sens. Lett. 7(4), 801–805 (2010)
4. Bourennane, S., Fossati, C., Cailly, A.: Improvement of target detection based on tensorial modelling (2010)
5. Cichocki, A., Zdunek, R., Phan, A., Amari, S.: Nonnegative matrix and tensor factorizations: applications to exploratory multi-way data analysis and blind source separation. Wiley, New Jersey (2009)
6. Daubechies, I.: Ten lectures on wavelets. SIAM (2006)
7. De Lathauwer, L., De Moor, B., Vandewalle, J.: A multilinear singular value decomposition. SIAM J. Matrix Anal. Appl. 21(4), 1253–1278 (2000)

8. De Lathauwer, L., De Moor, B., Vandewalle, J.: On the best rank-1 and rank-(r1, r2,..., rn) approximation of higher-order tensors. SIAM J. Matrix Anal. Appl. 21(4), 1324–1342 (2000)
9. Jin, X., Paswaters, S., Cline, H.: A comparative study of target detection algorithms for hyperspectral imagery. In: SPIE Defense, Security, and Sensing, p. 73341W–73341W. International Society for Optics and Photonics (2009)
10. Kerekes, J., Baum, J.: Hyperspectral imaging system modeling. Linc. Lab. J. 14(1), 117–130 (2003)
11. Kuybeda, O., Malah, D., Barzohar, M.: Rank estimation and redundancy reduction of high-dimensional noisy signals with preservation of rare vectors. IEEE Trans. Signal Process. 55(12), 5579–5592 (2007)
12. Letexier, D., Bourennane, S.: Noise removal from hyperspectral images by multidimensional filtering. IEEE Trans. Geosci. Remote Sens. 46(7), 2061–2069 (2008)
13. Letexier, D., Bourennane, S., Blanc-Talon, J.: Nonorthogonal tensor matricization for hyperspectral image filtering. IEEE Geosci. Remote Sens. Lett. 5(1), 3–7 (2008)
14. Lin, T., Bourennane, S.: Hyperspectral image processing by jointly filtering wavelet component tensor. IEEE Trans. Geosci. Remote Sens. 51(6), 3529–3541 (2013)
15. Manolakis, D., Marden, D., Shaw, G.A.: Hyperspectral image processing for automatic target detection applications. Linc. Lab. J. 14(1), 79–116 (2003)
16. Muti, D., Bourennane, S.: Multidimensional filtering based on a tensor approach. Signal Process. 85(12), 2338–2353 (2005)
17. Renard, N., Bourennane, S.: Improvement of target detection methods by multiway filtering. IEEE Trans. Geosci. Remote Sens. 46(8), 2407–2417 (2008)